Published in final edited form as:
Bioconjug Chem. 2010 March 17; 21(3): 436–444. doi:10.1021/bc9003102.

A dual-labeled knottin peptide for PET and near-infrared fluorescence imaging of integrin expression in living subjects

Richard H. Kimura[†], **Zheng Miao**[†], **Zhen Cheng**[†], **Sanjiv S. Gambhir**[†,‡], and **Jennifer R. Cochran**[†,*]

[†]Department of Radiology, Molecular Imaging Program, Stanford University, Stanford, CA 94305

[‡]Department of Bioengineering, Cancer Center, Bio-X Program, Stanford University, Stanford, CA 94305

Abstract

Previously, we used directed evolution to engineer mutants of the *Ecballium elaterium* trypsin inhibitor (EETI-II) knottin that bind to $\alpha_v\beta_3$ and $\alpha_v\beta_5$ integrin receptors with low nanomolar affinity, and showed that Cy5.5- or ^{64}Cu-DOTA-labeled knottin peptides could be used to image integrin expression in mouse tumor models using near-infrared fluorescence (NIRF) imaging or positron emission tomography (PET). Here, we report the development of a dual-labeled knottin peptide conjugated to both NIRF and PET imaging agents for multimodality imaging in living subjects. We created an orthogonally-protected peptide-based linker for stoichiometric coupling of ^{64}Cu-DOTA and Cy5.5 onto the knottin N-terminus, and confirmed that conjugation did not affect binding to $\alpha_v\beta_3$ and $\alpha_v\beta_5$ integrins. NIRF and PET imaging studies in tumor xenograft models showed that Cy5.5 conjugation significantly increased kidney uptake and retention compared to the knottin peptide labeled with ^{64}Cu-DOTA alone. In the tumor, the dual-labeled ^{64}Cu-DOTA/Cy5.5 knottin probe showed decreased wash-out leading to significantly better retention ($p < 0.05$) compared to the ^{64}Cu-DOTA-labeled knottin probe. Tumor uptake was significantly reduced ($p < 0.05$) when the dual-labeled probe was co-injected with an excess of unlabeled competitor and when tested in a tumor model with lower levels of integrin expression. Finally, plots of tumor-to-background tissue ratios for Cy5.5 versus ^{64}Cu uptake were well correlated over several time points post injection, demonstrating pharmacokinetic cross validation of imaging labels. This dual-modality NIRF/PET imaging agent is promising for further development in clinical applications where high sensitivity and high-resolution are desired, such as detection of tumors located deep within the body and image-guided surgical resection.

Introduction

The formation of new blood vessels that enable tumor growth is mediated in part by the differential expression or over-expression of various proteins. Among these are the integrin receptors, a family of heterodimeric cell surface receptors that bind extracellular matrix proteins to mediate cell attachment and signaling (1). There are currently over twenty different integrin subtypes known. In particular, $\alpha_v\beta_3$ and $\alpha_v\beta_5$ integrins have been shown to be over-expressed on many different types of tumors and the tumor neovasculature (2, 3). These integrins have been proposed to play a role in mediating tumor growth, angiogenesis,

*To whom correspondence should be addressed. 318 Campus Drive, The James H. Clark Center, Stanford CA, 94305-5439; Phone (650)724-7808, jennifer.cochran@stanford.edu.

Supporting Information Available:Characterization of compounds by reversed-phase HPLC and MALDI-TOF MS, serum stability of ^{64}Cu-DOTA/Cy5.5-conjugated knottin 2.5D, competition binding of knottin peptides to integrins expressed on tumor cells, and correlation analysis of Cy5.5 and ^{64}Cu biodistribution data. This material is available free of charge via the Internet at http://pubs.acs.org.

and metastasis, making them attractive targets for cancer therapy (4-6). In addition, diagnostic agents are critically needed to monitor disease progression and to help identify patients who will best respond to integrin-targeted treatments (7-9).

Multimodal molecular imaging has emerged as a powerful tool in cancer diagnosis, treatment, and management as well as in drug development (10, 11). Many clinical and preclinical imaging applications are based on positron emission tomography (PET), single-photon emission computed tomography (SPECT), near-infrared fluorescence imaging (NIRF), bioluminescence, magnetic resonance imaging (MRI), and ultrasound. Each imaging modality has its own unique strengths and limitations, thus, combinations of different imaging modalities are now being used to overcome these inherent limitations (10, 12). Dual-modality NIRF/PET tracers may find important clinical applications where high-resolution optical imaging is coupled with the sensitivity of nuclear imaging. For example, in tumor detection coupled with surgical procedures, the radionuclide component could initially be used to accurately map lesions that have grown deep within the body. When the radionuclide has sufficiently decayed, the optical mode could aid in image-guided surgery to precisely verify tumor margins during and following resection, using a minimally-invasive laparoscopic instrument equipped with a NIRF detection system.

In this study, we developed a dual-modality NIRF/PET imaging agent based on the engineered integrin-binding knottin peptide 2.5D, which binds to $\alpha_v\beta_3$ and $\alpha_v\beta_5$ integrin receptors with high affinity (13). Cy5.5 and ^{64}Cu-1,4,7,10-tetra-azacyclododecane-N,N′,N″,N‴-tetraacetic acid (^{64}Cu-DOTA), were both chemically conjugated to the knottin N-terminus using a peptide-based linker that contained orthogonal protecting groups for sequential and precise coupling. We measured the integrin binding affinity and specificity of the dual-labeled ^{64}Cu-DOTA/Cy5.5 knottin peptide compared to unlabeled knottin peptide and peptides conjugated only to ^{64}Cu-DOTA or Cy5.5. Next, we used NIRF and PET imaging to evaluate tumor uptake, pharmacokinetics, and biodistribution of the dual-labeled ^{64}Cu-DOTA/Cy5.5 knottin peptide in human tumor xenograft models and compared these results to imaging studies performed with knottin peptides conjugated to only to ^{64}Cu-DOTA or Cy5.5. Compared to ^{64}Cu-DOTA, the hydrophobic Cy5.5 dye had a dramatic effect on probe pharmacokinetics and tissue biodistribution, with robust imaging signals lasting well beyond 24 hours. In addition to generating a dual-modality NIRF/PET imaging agent, the cross-linking strategy presented here could be useful in creating other multimodal imaging agents, as well as in creating molecules for theranostic applications that combine imaging diagnostics with therapy.

Experimental Procedures

Materials, Cell Lines, and Reagents

All 9-fluorenylmethyloxycarbonyl (Fmoc) protected amino acids were purchased from Novabiochem/EMD Chemicals Inc (La Jolla, CA) with the exception of Fmoc-N-ε-1-(4,4-dimethyl-2,6-dioxocyclohex-1-ylidene)-3-methylbutyl-L-lysine (Fmoc-Lys(ivDde)-OH) which was purchased from Bachem (Torrance, CA) and Fmoc-L-Tyr(tBu)-Wang Resin which was purchased from CS Bio Company (Menlo Park, CA). The U87MG human glioblastoma cell line was obtained from American Type Culture Collection (Manassas, VA). Detergent-solubilized $\alpha_v\beta_3$, $\alpha_v\beta_5$ integrin receptors (both octyl-beta-D-glucopyranoside formulations) and $\alpha_5\beta_1$ integrin (Triton X-100 formulation) were purchased from Millipore (Billerica, MA), and $\alpha_{iib}\beta_3$ (Triton X-100 formulation) was purchased from Enzyme Research Laboratories (South Bend, IN). ^{125}I-labeled echistatin and the backbone cyclized pentapeptide c(RGDyK) were purchased from Amersham/GE Healthcare (Piscataway, NJ), and Peptides International (Louisville, KY), respectively. Phosphate buffered saline (PBS) was from Gibco/Invitrogen (Carlsbad, CA). All other chemicals were

purchased from Thermo Fisher Scientific (Pittsburgh, PA) unless otherwise specified. Integrin binding buffer (IBB) was composed of 25 mM Tris pH 7.4, 150 mM NaCl, 2mM $CaCl_2$, 1 mM $MgCl_2$, 1 mM $MnCl_2$, and 0.1% bovine serum albumin (BSA).

Knottin Peptide Synthesis and Folding

Knottin peptides were synthesized on a CS Bio CS336 instrument using Fmoc-based solid phase peptide synthesis with Rink amide resin (CS Bio Company). Fmoc groups were removed with 20% piperidine in *N,N*-dimethylformamide (DMF). Amino acid coupling was performed using HOBt/diisopropylcarbodiimide chemistry in DMF. After synthesis, side-chain deprotection and resin cleavage was achieved by addition of a 94:2.5:2.5:1 (v/v) mixture of trifluoroacetic acid(TFA):triisopropylsilane:ethanedithiol:water for 2 h at room temperature. The crude product was precipitated with cold anhydrous diethyl ether, and purified by reversed-phase HPLC using a Varian Prostar instrument and Vydac C_{18} columns. Linear gradients of 90% acetonitrile in water containing 0.1% (v/v) TFA were used for all peptide purifications, which were monitored at an absorbance of 220 nm. Peptide purity was analyzed by analytical scale reversed-phase HPLC using a Vydac C_{18} column. Molecular masses were determined by matrix-assisted laser desorption/ionization time-of-flight mass spectrometry (MALDI-TOF MS) on a Perseptive Voyager-DE-RP Biospectrometry instrument (Stanford Protein and Nucleic Acid facility). Folding reactions were performed by incubating peptides with 2.5 mM reduced glutathione and 20% dimethlysulfoxide (v/v) in 0.1 M ammonium bicarbonate, pH 9 with gentle rocking overnight. The final oxidized product was purified by reversed-phase HPLC as described above and lyophilized. Purified peptides were dissolved in water, and concentrations were determined by amino acid analysis (AAA Service Laboratory, Damascus, OR). Peptide purity and molecular masses were determined by analytical scale reversed-phase HPLC and MALDI-TOF MS.

Synthesis of the Chemical Linker, Fmoc-Lys(ivDde)-Gly-Gly-Tyr-N-Hydroxysuccinimide Ester

Fmoc-Lys(ivDde)-Gly-Gly-Tyr was synthesized as described above using a preloaded Fmoc-L-Tyr(tBu)-Wang resin and Fmoc-Lys(ivDde)-OH. This peptide was cleaved from the resin and was purified as described above, leaving the Fmoc and ivDde protecting groups attached. The C-terminal carboxyl group of the peptide was activated as an NHS ester by reaction with *N, N′*-dicyclohexylcarbodiimide (DCC; Pierce Chemical Company, Rockford, IL) and N-hydroxysuccinimide (NHS) in DMF, and was purified by reversed-phase HPLC to yield Fmoc-Lys(ivDde)-Gly-Gly-Tyr-NHS ester.

Chemical Conjugation of Cy5.5 and DOTA

Knottin peptide 2.5D was reacted with Fmoc-Lys(ivDde)-Gly-Gly-Tyr-NHS ester in DMF containing 2% *N,N*-diisopropylethylamine (DIEA) to yield Fmoc-Lys(ivDde)-Gly-Gly-Tyr-2.5D. The Fmoc-group was then removed by incubating this intermediate in DMF with 10% piperidine for 0.5 hr to yield NH_2-Lys(ivDde)-Gly-Gly-Tyr-2.5D. This intermediate was reacted with a 5-fold molar excess of an NHS ester-activated DOTA group (DOTA-NHS ester; Macrocyclics, Dallas, TX) in DMF containing 2% DIEA for 0.5 hr to yield DOTA-Lys(ivDde)-Gly-Gly-Tyr-2.5D. Next, the ivDde group was removed by incubation in DMF containing 2% hydrazine (Alfa Aesar, Ward Hill, MA) for 0.5 hr at room temperature. Finally, DOTA-Lys(NH_2)-Gly-Gly-Tyr-2.5D was reacted with an excess of Cy5.5-NHS ester (Amersham) in DMF containing 2% DIEA for 0.5 hr at room temperature to yield DOTA-Lys(Cy5.5)-Gly-Gly-Tyr-2.5D. Following each step, the intermediates were purified by reversed-phase HPLC. Molecular masses were determined by MALDI-TOF MS

and peptide products were analyzed by analytical scale reversed-phase HPLC as described above (Supporting Information; Figure S1).

^{64}Cu radiolabeling

For each radiolabeling reaction, approximately 10-25 μg DOTA-Lys(Cy5.5)-Gly-Gly-Tyr-2.5D was incubated with 1-2 mCi $^{64}CuCl_2$ (University of Wisconsin-Madison, Madison, WI) in 0.1 N sodium acetate (pH 6.3) for 1 hr at 42 °C. The reaction was terminated with the addition of EDTA. ^{64}Cu-DOTA-Lys(Cy5.5)-Gly-Gly-Tyr-2.5D was purified using a PD-10 column (Amersham Biosciences/GE Healthcare) and eluted with PBS (pH 7.4), and passed through a 0.22 μm filter for animal experiments. The radiochemical purity, determined as the ratio of the main product peak to other peaks, was determined by HPLC to be > 95%. The radiochemical yield, determined as the ratio of final activity of the product over the starting activity used for the reaction, was usually over 80%. The specific activity of the probe was ∼500 Ci/mmol.

Cell Surface Integrin Receptor Binding and Uptake Assays

Cell surface competition binding assays were performed as previously described (14, 15). Briefly, 2×10^5 U87MG cells were incubated with 0.06 nM ^{125}I-labeled echistatin (Amersham) and varying concentrations of peptides in IBB at room temperature for 3 hr. The cell-bound radioactivity remaining after washing was measured by scintillation counting. Half-maximal inhibitory competition (IC_{50}) values were determined by non-linear regression analysis using Kaleidagraph (Synergy Software), and are presented as the average of experiments performed on three separate days.

For cell uptake studies, 5×10^5 U87MG or MDA-MB-435 cells were suspended in 50 μL IBB and incubated with ^{64}Cu-DOTA/Cy5.5-2.5D (1.5 μCi/tube in 100μL IBB) with or without 1 μ*g* of c(RGDyK) at 37 °C for 30, 60, and 120 min. Cells were then washed three times with chilled PBS and pelleted by centrifugation. The radioactivity of the cell pellet was measured using a gamma counter (PerkinElmer 1470, Waltham, MA). Cell binding and uptake of ^{64}Cu-DOTA/Cy5.5-2.5D was expressed as the percentage of added radioactivity. Experiments were performed in triplicate.

Solid Phase Integrin Receptor Competition Binding Assay

Integrin receptor competition binding assays were performed as previously described (15, 16). Briefly, detergent-solubilized $\alpha_v\beta_3$, $\alpha_v\beta_5$, $\alpha_5\beta_1$, or $\alpha_{iib}\beta_3$ integrin receptors were diluted to a final concentration of 1 μg/mL in IBB, and 100 μL aliquots were used to coat wells of Maxisorb plates (NalgeNunc, Thermo Fisher Scientific), overnight at 4 °C. The wells were washed and blocked with IBB containing 1% BSA for 2 h at room temperature. ^{125}I-labeled echistatin (0.06 nM) and varying concentrations of unlabeled peptides were incubated in the wells for 3 hr at room temperature with gentle rocking, and washed 3 times in IBB. Plate-bound radioactivity was solubilized with 200 μL of boiling 2N NaOH followed by gamma-counting. Each data point represents the average value of triplicate wells, and error bars represent the standard deviation.

Tumor Xenograft Models

U87MG glioblastoma cells and MDA-MB-435 melanoma cells were maintained at 37 °C in a humidified atmosphere containing 5% CO_2 in Dulbecco's Modified Eagle Medium or Leibovitz L-15 Medium, respectively, containing 10% heat-inactivated fetal bovine serum and penicillin-streptomycin (all from Invitrogen). Animal procedures were carried out according to a protocol approved by Stanford University Administrative Panels on Laboratory Animal Care. Female athymic nude mice (nu/nu), obtained at 4-6 weeks of age

(Charles River Laboratories, Inc., Wilmington, MA), were injected subcutaneously in the right or left shoulder with $\sim 10^7$ U87MG or 5×10^6 MDA-MB-435 cells suspended in 100 μL of PBS. Mice were used for *in vivo* imaging studies when their tumors reached approximately 8 to 10 millimeters in diameter.

Near-Infrared Fluorescence and MicroPET Imaging of Tumor Xenografts

NIRF imaging was performed with an IVIS 200 (Xenogen, Hopkinton, MA) as previously described (14). Briefly, a Cy5.5 filter set was used and fluorescence emission was normalized to photons per second per centimeter squared per steradian ($p/s/cm^2/sr$). Images were acquired and analyzed using Living Image 2.50.1 (Xenogen). For all experiments, U87MG tumor-bearing mice (n = 3 for each probe) were injected via tail vein with ∼1.5 nmol of probe in 100 μL PBS and imaged at various times post injection. Tumor contrast was quantified by drawing identically-sized regions of interest (ROI) around the tumor and background tissue located in the mouse's flank (average radiance, $p/s/cm^2/sr$). Data points represent the average tumor/tissue ratio for a group of three animals.

U87MG or MDA-MB-435 tumor-bearing mice (n = 3 or more for each probe) were injected with ∼100 μCi (∼0.5 nmol) of probe via the tail vein and imaged with a microPET R4 rodent model scanner (Siemens Medical, Knoxville, TN) using 3 or 5 min static scans. Images were reconstructed by a two dimensional ordered expectation maximum subset algorithm and calibrated as previously described (17). ROIs were drawn over the tumor on decay-corrected whole body images using ASIPro VM software (Siemens Medical). The mean counts per pixel per minute were obtained from the ROI and converted to counts per milliliter per minute with a calibration constant. ROIs were converted to counts/g/min, and %ID/g values were determined assuming a tissue density of 1 g/mL. No attenuation correction was performed. In NIRF and PET blocking experiments, mice were co-injected with 330 μg (∼0.5 μmol) of unlabeled c(RGDyK). For whole animal NIRF/PET correlation plots, the average tumor-to-background tissue ratios were determined using an ROI over tumor tissue and dividing by an ROI over the thigh area for three mice per time point post injection. Linear regression analysis in Microsoft Excel was used to determine the R^2 value, and error bars represent the standard deviation.

In Vivo Biodistribution Studies

Anesthetized nude (nu/nu) mice bearing U87MG tumor xenografts were injected with ∼100 μCi (∼0.5 nmol) of ^{64}Cu-DOTA-Lys(Cy5.5)-Gly-Gly-Tyr-2.5D via the tail vein, and were euthanized at 1, 4, and 24 hr post injection. Blood, bone, brain, heart, kidney, liver, lung, muscle, pancreas, skin, spleen, and tumor tissue were removed and weighed. The fluorescence flux (photons per second) or gamma emissions (counts per minute) of the tissue were measured by fluorescence imaging or by gamma counting, respectively. For the fluorescence component, the results are expressed as flux/gram of tissue and represent the mean and standard deviation of experiments performed on three mice. Total flux was determined for dissected tissue by drawing a ROI around the entire tissue and subtracting the total background flux from an adjacent equally-sized ROI. For studies involving radioactivity, the results were expressed as the percent injected dose per gram (%ID/g) of tissue and represent the mean and standard deviation of experiments performed on three mice. For each mouse, the activity of tissue samples was calibrated against a pre-measured aliquot of the radio-tracer and normalized to the whole bodyweight and to the residual radioactivity present in the tail. For correlation analysis of biodistribution data from three mice, average Cy5.5 tumor-to-tissue ratios were plotted versus average ^{64}Cu tumor-to-tissue ratios for 1, 4, and 24 hr time points. Linear regression analysis in Microsoft Excel was used to determine the R^2 value, and error bars represent the standard deviation.

In Vivo Metabolite Analysis

For metabolite analysis, anesthetized nude (nu/nu) mice bearing U87MG tumor xenografts were injected with 200-400 μCi of ^{64}Cu-DOTA-Lys(Cy5.5)-Gly-Gly-Tyr-2.5D via the tail vein, and were euthanized at 1, 4, or 24 hr post injection. Blood, liver, kidney and tumor tissue were removed and suspended in ∼500 μL PBS. An additional 500-1000 μl DMF was added and the tissues were homogenized with a mortar and pestle. The homogenate was filtered using a Costar Spin-X (Corning, Lowell, MA) 0.2 μm nylon microcentrifuge filter to isolate soluble metabolites. The filtrates were analyzed by reversed-phase HPLC. Eluted fractions were collected in 30 sec intervals and a gamma counter was used to determine counts per minute (cpm).

Statistical Analysis

All data are presented as the average value ± the SD of n independent measurements. Statistical analysis for animal studies and binding studies were performed by two factor ANOVA without replication analysis using Microsoft Excel. Significance was assigned for p values of <0.05.

Results

Synthesis and Characterization of a Knottin Peptide Conjugated to Both DOTA and Cy5.5

To create a dual-modality NIRF/PET imaging agent, we developed a chemical strategy to couple both ^{64}Cu-DOTA and Cy5.5 to an engineered knottin peptide (knottin 2.5D), which binds to $\alpha_v\beta_3$ and $\alpha_v\beta_5$ integrin receptors with low nanomolar affinity (13). A peptide-based linker (Fmoc-Lys(ivDde)-Gly-Gly-Tyr-NHS ester) enabled stochiometric chemical coupling of these two different imaging labels specifically to the knottin N-terminus. The conjugation chemistry is shown in Scheme 1. Fmoc-Lys(ivDde)-Gly-Gly-Tyr was first treated with DCC/NHS to activate the C-terminal carboyxlate and generate a reactive succinimide ester group. The tyrosine residue appeared to stabilize the succinimide ester intermediate and afforded a convenient handle for peptide detection and quantification by absorbance at 280 nm. This linker was coupled to the N-terminus of knottin 2.5D through formation of a peptide bond. The Fmoc and the ivDde groups were then selectively and sequentially removed to allow precise coupling of DOTA to the N-terminal amine and Cy5.5 to the ε-amino group of the lysine residue. Each reaction intermediate was purified by reversed-phase HPLC and the correct mass was verified by MALDI-TOF MS (Supporting Information; Figure S1). To reduce sample loss associated with purification, we subsequently found that the ivDde de-protection step could be performed in the same reaction vessel used to couple the DOTA group. Next, the resulting integrin-binding knottin bioconjugate (termed DOTA-Lys(Cy5.5)-Gly-Gly-Tyr-2.5D) was radiolabeled with ^{64}Cu through chelation with the DOTA group. We measured the stability of ^{64}Cu-DOTA-Lys(Cy5.5)-Gly-Gly-Tyr-2.5D upon exposure to mouse serum. Radio-HPLC analysis indicated minimal probe degradation after incubation in a solution of 50% mouse serum for 1 hr at 37 °C (Supporting Information; Figure S2). Degradation levels increased over time and intact probe was unrecoverable after incubation in serum for 24 hr.

Binding of the DOTA/Cy5.5-Conjugated Knottin Peptide to Integrin-Expressing Tumor Cells

To test if conjugation of Cy5.5 and DOTA to the knottin N-terminus affected its ability to bind to integrin receptors, we measured the ability of DOTA-Lys(Cy5.5)-Gly-Gly-Tyr-2.5D to compete with ^{125}I-labeled echistatin for binding to U87MG glioblastoma cells. Echistatin, a polypeptide from snake venom, has a K_D of approximately 0.4 nM for $\alpha_v\beta_3$ integrin (18). For comparison, we also measured the relative binding affinities of knottin peptide 2.5D

with DOTA or Cy5.5 groups conjugated directly to the N-terminus. All knottin peptides were shown to bind in a dose-dependent matter to U87MG cells. The half-maximal inhibitory concentration (IC_{50}) values of DOTA/Cy5.5-conjugated knottin 2.5D and unlabeled knottin 2.5D were 30 ± 7 nM and 19 ± 6 nM (15), respectively, which were not statistically different ($p < 0.23$) (Table 1). In contrast, the relative binding affinities of DOTA-conjugated knottin 2.5D (IC_{50} = 9 ± 3 nM), and Cy5.5-lableled knottin 2.5D (IC_{50} = 5 ± 1 nM) were statistically significant compared to DOTA/Cy5.5-conjugated knottin 2.5D ($p < 0.05$). These results indicate that integrin binding affinity is relatively unaffected by the addition of both Cy5.5 and DOTA through a flexible peptide linker. The binding isotherms of all of these compounds are shown in Supporting Information Figure S3 to facilitate direct comparison.

Integrin Binding Specificity of the DOTA/Cy5.5-Conjugated Knottin Peptide

We next tested whether conjugation of both Cy5.5 and DOTA to the N-terminus of knottin 2.5D affected its integrin binding specificity. Since U87MG cells have been shown to express $\alpha_v\beta_5$, and $\alpha_5\beta_1$ integrins in addition to $\alpha_v\beta_3$ integrin (19), we measured integrin binding specificity by competition of ^{125}I-echistatin to detergent-solubilized $\alpha_v\beta_3$, $\alpha_v\beta_5$, $\alpha_5\beta_1$, or $\alpha_{iib}\beta_3$ integrin receptors coated onto microtiter plates. Unlabeled echistatin was used as a positive control since it has been previously shown to bind to all four receptors with high affinity (13, 20). DOTA-Lys(Cy5.5)-Gly-Gly-Tyr-2.5D exhibited strong binding to $\alpha_v\beta_3$ and $\alpha_v\beta_5$ integrins, modest binding to $\alpha_5\beta_1$ integrin, and weak binding to $\alpha_{iib}\beta_3$ integrin (Figure 1). In comparison, similar results were observed with unlabeled knottin 2.5D and DOTA-conjugated knottin 2.5D (15). However, knottin peptide 2.5D labeled directly at its N-terminus with Cy5.5 showed increased binding to integrin receptors compared to the other knottin peptides we tested (Table 1 and Figure 1). This increase in binding was statistically significant for all data points compared to unlabeled knottin 2.5D ($p < 0.05$), and could be due to the close proximity of the hydrophobic Cy5.5 dye molecule to the integrin binding epitope. Interestingly, this effect was not observed with the dual-labeled knottin, which has its Cy5.5 and DOTA groups conjugated through the peptide-based linker and not directly at the knottin N-terminus (Figure 1). Cy5.5-labeled peptides, such as the backbone cyclized pentapeptide c(RGDyK), have also shown increased integrin binding affinities compared to unmodified compounds (14).

In Vivo Near-Infrared Fluorescence Imaging with the DOTA/Cy5.5-Conjugated Knottin Peptide

We tested the ability of the DOTA/Cy5.5-labeled knottin peptide to target tumors in living subjects to evaluate its potential as an *in vivo* molecular imaging agent. Figure 2A shows typical NIRF images of athymic nude mice bearing subcutaneous U87MG glioblastoma tumors after tail vein injection of 1.5 nmol of the DOTA/Cy5.5-conjugated knottin peptide. DOTA-Lys(Cy5.5)-Gly-Gly-Tyr-2.5D generated increasing tumor-to-background tissue ratios of 2.96 ± 0.42, 3.11 ± 0.66, 3.60 ± 0.84, and 4.04 ± 0.34 at 1, 2, 4, and 24 hr post injection, respectively (Figure 2C). In comparison, knottin peptide 2.5D labeled directly at its N-terminus with Cy5.5 also generated similar signals 1, 2, and 4 hr post injection (2.09 ± 0.61, 2.57 ± 0.79, and 3.99 ± 0.55, respectively), which persisted at the 24 hr time point (4.47 ± 0.39) (15). Co-injection of a molar excess of unlabeled c(RGDyK) significantly decreased uptake of DOTA-Lys(Cy5.5)-Gly-Gly-Tyr-2.5D, particularly at later time points ($p < 0.05$) (Figure 2B). At 1 hr post injection, the tumor-to-background tissue ratio generated by this mixture was 2.16 ± 0.15, and did not increase to any significant extent at later time points (2.47 ± 0.34 at 24 hr) (Figure 2C). This background signal is similar to that observed in other studies with Cy5.5-labeled peptides, including a negative control Cy5.5-labeled knottin peptide we previously tested (14, 15).

MicroPET Imaging of U87MG Xenografts with the ^{64}Cu-DOTA/Cy5.5-Conjugated Knottin Peptide

We tested the potential of the ^{64}Cu-DOTA/Cy5.5-labeled knottin peptide for use as a PET imaging probe in mice bearing U87MG human tumor xenografts. ^{64}Cu-DOTA-Lys(Cy5.5)-Gly-Gly-Tyr-2.5D rapidly accumulated at the tumor site and persisted there throughout the course of the experiment (Figure 2D). We observed tumor uptake values of 4.27 ± 0.46, 4.19 ± 0.36, 4.52 ± 0.31 and 5.02 ± 0.05 %ID/g at 1, 2, 4, and 24 hr post injection, respectively (Figure 2F). In contrast, knottin peptide 2.5D labeled directly at its N-terminus with ^{64}Cu-DOTA generated similar tumor uptake values at the 1 hr time point (4.47 ± 1.21 %ID/g), but exhibited significantly faster wash-out (1.48 ± 0.51 %ID/g at 24 hr). Tumor uptake of ^{64}Cu-DOTA-Lys(Cy5.5)-Gly-Gly-Tyr-2.5D was significantly decreased ($p < 0.05$) by co-injection of ∼ 0.5 μmol of unlabeled c(RGDyK) (Figure 2E), resulting in values of approximately 1-1.5 %ID/g from 1 to 24 h post injection (Figure 2F).

A plot of tumor-to-background tissue ratios for NIRF versus PET imaging showed good linear correlation ($R^2 = 0.85$) over 1 - 24 hr, indicating that the two labels are effectively delivered to the tumor, and can be detected by both imaging modalities over the time course of the experiment (Figure 2G). A direct 1:1 correlation is not observed due to inherent differences in the background tissue measured with each non-invasive *in vivo* imaging technique. More specifically, although the depth of fluorescence light penetration is several millimeters into the muscle, the background signal quantified by NIRF imaging results mainly from high autofluorescence of the skin. In contrast, the background signal obtained in microPET imaging is quantified on the muscle tissue.

Comparative Cell Uptake and MicroPET Imaging in MDA-MB-435 Xenografts

To further confirm integrin specificity, we tested binding and uptake of ^{64}Cu-DOTA-Lys(Cy5.5)-Gly-Gly-Tyr-2.5D in two cell lines: U87MG and MDA-MB-435, a melanoma cell line which expresses 2×10^4 integrin receptors, compared to approximately 1×10^5 integrin receptors expressed on U87MG cells (21). As expected, lower levels of probe uptake was observed over time in MDA-MB-435 versus U87MG cells, correlating with their lower levels of integrin receptor expression (Figure 3A). In both cell lines, binding and uptake was blocked by addition of an excess of c(RGDyK). Consistent with these results, tumor uptake of ^{64}Cu-DOTA-Lys(Cy5.5)-Gly-Gly-Tyr-2.5D in MDA-MB-435 xenograft models was much lower compared to uptake in U87MG tumors, exhibiting values of 1.33 ± 0.02 %ID/g and 1.01 ± 0.10 %ID/g at 1 and 24 hr post injection (Figure 3B). Furthermore, MDA-MB-435 tumor uptake was significantly decreased to 0.82 ± 0.05 %ID/g and 0.60 ± 0.09 %ID/g at 1 and 24 hr post injection ($p < 0.05$) upon co-injection of a molar excess of unlabeled c(RGDyK).

Biodistribution Studies of ^{64}Cu-DOTA/Cy5.5- and DOTA/Cy5.5-Conjugated Knottin Peptides

We determined the tissue biodistribution of DOTA/Cy5.5- and ^{64}Cu-DOTA/Cy5.5-conjugated knottin peptides in U87MG tumor-bearing mice using fluorescence and radioactivity measurements. Mice were injected with DOTA-Lys(Cy5.5)-Gly-Gly-Tyr-2.5D and fluorescent images of individual organs were obtained at various time points. In these studies, DOTA/Cy5.5-conjugated knottin 2.5D accumulated rapidly at the tumor site at early time points and decreased over time with fluorescence flux/gram values of 373.1 ± 111.3 and 146.1 ± 26.5 for 1 and 24 hr post injection, respectively (Figure 4A). Next, mice were injected with ^{64}Cu-DOTA-Lys(Cy5.5)-Gly-Gly-Tyr-2.5D and individual organs were analyzed by gamma counting. For tumor tissue, we observed biodistribution values of 3.24 ± 0.87, 5.64 ± 0.83 and 4.57 ± 0.70 %ID/g at 1, 4, and 24 hr post injection, respectively (Figure 4B). Higher liver uptake (∼4-7 % ID/g at 1 and 4 hr) and kidney uptake (∼80 %ID/

g for 1-4 hr) were observed compared to other organs (Figure 4B and 5B). Kidney uptake was reduced at 24 hr (~30 %ID/g) in both Cy5.5 and ^{64}Cu biodistribution studies (Figure 5).

To further compare the DOTA/Cy5.5- and ^{64}Cu-DOTA/Cy5.5-knottin biodistribution data, tumor-to-tissue ratios were calculated (Figure 4C-D). In general, the tumor-to-blood and tumor-to-muscle ratios were slightly higher for fluorescence imaging (Cy5.5 uptake) compared to radioactivity measurements (^{64}Cu uptake). This trend was also observed for the tumor-to-tissue ratios for the liver, lung, and spleen. Plots of tumor-to-background tissue ratios for Cy5.5 versus ^{64}Cu uptake in various organs showed good correlation, with an intercept of zero and R^2 values of 0.75, 0.83, and 0.82 for 1, 4, and 24 hr post injection, respectively, demonstrating relatively uniform distribution of imaging labels in tumors and off-target tissues (Supporting Information; Figure S4). The high tumor-to-blood ratios and high tumor-to-muscle-ratios observed at 1, 4, and 24 hr post injection suggest that ^{64}Cu-DOTA-Lys(Cy5.5)-Gly-Gly-Tyr-2.5D may be useful for whole body radiographic imaging where the tumor signal is not obscured by a strongly emitting background signal from non-targeted organs.

Metabolic Stability

Finally, we tested the *in vivo* stability of ^{64}Cu-DOTA-Lys(Cy5.5)-Gly-Gly-Tyr-2.5D. The metabolic breakdown of probe was examined after recovery from whole mouse blood, tumor, liver, and kidney 1 hr post injection. The radioactivity recovered in the soluble tissue extract ranged from 50-80% compared to the insoluble cellular debris or pellet fraction. This soluble extract was filtered and separated by reversed-phase HPLC, and fractions were analyzed by gamma counting. The dual-labeled ^{64}Cu-DOTA/Cy5.5 knottin peptide appeared to have similar stability in serum and blood after 1 hr incubation (Figure 6 and Supporting Information; Figure S2). In contrast, significant breakdown of probe was seen in the tumor, and intact probe was not able to be recovered from the liver and kidney. In these samples, metabolites with retention times between 3 to 6 minutes were present at high levels.

Discussion

A chemical cross-linking strategy was developed to couple two complementary molecular imaging agents onto a disulfide-rich knottin peptide that has been engineered to bind to $\alpha_v\beta_3$ and $\alpha_v\beta_5$ integrins with high affinity. The folding of cystine knot peptides is highly dependent on primary structure (22). We observed that simple N-terminal acetylation or biotinylation of EETI-II severely affected its ability to properly fold, consistent with another study on permutants of the cyclotide kalata B1 (23). These stringent folding requirements dictated that all conjugation chemistry be performed in solution after the knottin was folded, instead of using on-bead labeling of side-chain protected linear peptides immediately following synthesis. Therefore, we used a cross-linking strategy that selectively and sequentially exposed reactive groups for precise, stoichiometric coupling of both an optical imaging dye and a radiochelator to the knottin N-terminus. The method we developed is flexible, and can be used to accommodate a variety of imaging labels, therapeutics, or pharmacokinetic modulators for diverse biomedical applications. Importantly, we demonstrated that attachment of several chemical groups to the N-terminus of the engineered EETI-II knottin peptide did not interfere with its ability to bind to integrin receptors with high affinity.

Stability studies showed that the ^{64}Cu-DOTA-Lys(Cy5.5)-Gly-Gly-Tyr-2.5D probe is relatively labile, both in high concentrations of serum and after injection into the body. This breakdown is most likely due to proteolysis of the cross-linking moiety as we previously showed that knottin peptide ^{64}Cu-DOTA-2.5D exhibited only minimal fragmentation after

incubation in serum for 24 h, and was recovered intact from the blood, tumor, and kidneys 1 hr after injection into mice (15). Given that similar maximal tumor uptake levels were observed from ^{64}Cu-DOTA-2.5D and ^{64}Cu-DOTA-Lys(Cy5.5)-Gly-Gly-Tyr-2.5D, this proteolysis did not appear to affect its rapid tumor accumulation. However, degradation could have influenced kidney uptake and retention of dye molecules or metals. Cross-linkers composed of non-natural amino acids or peptoids may facilitate a more stable linkage (24). In addition, the use of D-amino acids has been shown to stabilize a variety of imaging peptides such as somatostatin (25). We are currently using these strategies to create more stable cross-linkers for the development of theranostic agents that will apply molecular imaging to quantify the delivery of cytotoxic drugs to tumors.

The use of a dual-labeled agent has distinct advantages as opposed to co-administering separate single-labeled agents. Having both labels on the same affinity ligand allows pharmacokinetic quantification of a single compound. This is beneficial because, as our study showed, the hydrophobic Cy5.5 dye strongly influenced the pharmacokinetics and tissue biodistribution of the radionuclide imaging agent. In addition, dual labeling allows quantitative cross validation and direct comparison between nuclear and optical imaging using an affinity ligand (26). Several groups have developed dual-labeled NIRF/SPECT probes using near-infrared dyes and ^{111}In or ^{99m}Tc radiolabels (26-31); these probes are specific to a variety of disease targets and have been recently reviewed (32). Studies describing chemically-defined, dual-labeled NIRF/PET probes have been more limited. NIRF/PET probes have been developed by decorating quantum dots with tumor targeting moieties and radiolabeling the resulting nanoparticles with ^{64}Cu (33, 34). Compared to our knottin peptides, these nanoparticles exhibited extremely high uptake in the liver, spleen, lymph nodes, and bone marrow.

Addition of Cy5.5 had both a positive and negative effect on the pharmacokinetics and biodistribution of the probe. In comparison to ^{64}Cu-DOTA-2.5D, which rapidly washed out of the tumor, ^{64}Cu-DOTA-Lys(Cy5.5)-Gly-Gly-Tyr-2.5D was significantly retained by the tumor at later time points (Figure 2D). This tumor uptake was specific and mediated by integrin receptors as demonstrated by blocking experiments with c(RGDyK), which interacts with the same integrin binding site as the engineered knottin peptides (Figure 2), as well as the lower levels of tumor uptake in MDA-MB-435 tumors, which express lower levels of integrin receptors compared to U87MG tumors (Figure 3). Moreover, in previous studies we used knottin peptides containing a scrambled sequence to validate the integrin binding specificity of ^{64}Cu-DOTA- and Cy5.5-labeled knottin probes (13, 15).

Cy5.5 rapidly accumulated in the kidneys over the course of the imaging experiments (Figure 2A and 5A), consistent with the high levels of kidney uptake and retention we observed with knottin peptide 2.5D labeled only with Cy5.5 (15). In our previous studies, the kidney uptake for ^{64}Cu-DOTA-2.5D was 8.08 ± 0.67, 2.69 ± 0.48, and 1.25 ± 0.11 %ID/g at 1, 4, and 24 hr post injection, respectively (15). In contrast, kidney uptake for ^{64}Cu-DOTA-Lys(Cy5.5)-Gly-Gly-Tyr-2.5D was 78.4 ± 13.9 and 80.9 ± 14.9 %ID/g for 1 hr and 4 hr post injection; however, after 24 hr the radioactivity in the kidneys decreased to 32.2 ± 2.2 %ID/g, suggesting that ^{64}Cu metabolites are cleared by the kidneys at later time points. This decrease in kidney signal is not due to the short half-life of ^{64}Cu (12.7 hr), as the data has been normalized to account for radioactive decay. Liver uptake (∼ 4-7 %ID/g at 1-24 hr post injection) was also higher then previously observed for ^{64}Cu-DOTA-2.5D, in which values of ∼1-2 %ID/g were observed 1 to 4 hr post injection. Increased liver and kidney uptake may preclude the use of this probe to identify lesions located in the abdomen; however, the spatial resolution of PET imaging, which is in the millimeter range, may allow identification of small lesions in close proximity to these organs. In addition, while kidney uptake and retention was high from Cy5.5-labeled probes, in future studies the use of

alternate fluorescent dyes with more favorable biodistribution properties may help address this issue. Small amounts of probe are used for imaging applications, thus, we do not expect this probe to be immunogenic. However, as with any new compound intended for clinical use, this will have to be determined empirically.

In summary, the cross-linking strategy we describe here has broad applicability for site-specific coupling of two different imaging labels, or an imaging label and a therapeutic moiety, to knottin peptides for cancer diagnosis or therapy, or both. Conjugation of a tumor-specific knottin peptide to both a PET imaging agent and a chemotherapeutic agent could allow simultaneous and quantitative measurement of biodistribution and pharmacokinetics, drug delivery to tumors, and tumor response during the course of treatment. Moreover, different combinations of imaging labels may yield additional or unique information during a multimodal scan. The molecular tools developed here will allow research in these areas to be explored.

Supplementary Material

Refer to Web version on PubMed Central for supplementary material.

Acknowledgments

We thank Adam Silverman, Bryan Smith, and Douglas Jones for helpful discussions and critical feedback, Fred Chin and David Dick in the Stanford Cyclotron Facility, and Tim Doyle, Laura Pisani, and Frezghi Habte in the Stanford Small Animal Imaging Facility. We also thank Edwin Chang for providing the MDA-MB-435 mouse xenograft models. This work was funded by the NIH National Cancer Institute (NCI) Howard Temin Award 5K01 CA104706 and the Mallinckrodt Faculty Scholar Award (to J.R.C.), NIH ICMIC P50 CA114747, NCI 5R25 CA118681, and the Canary Foundation (to S.S.G.), and a Stanford Molecular Imaging Scholars postdoctoral fellowship R25 CA118681 (to R.H.K.).

Abbreviations

EETI-II	*Ecballium elaterium* trypsin inhibitor
DOTA	1,4,7,10-tetra-azacyclododecane-N,N′,N″,N‴-tetraacetic acid
NIRF	near-infrared fluorescence
PET	positron emission tomography
RGD	arginine-glycine-aspartic acid
SPECT	single-photon emission computed tomography
MRI	magnetic resonance imaging
CT	computed tomography
Fmoc	9-fluorenylmethyloxycarbonyl
PBS	phosphate buffered saline
IBB	integrin binding buffer
BSA	bovine serum albumin
DMF	*N*,*N*-dimethylformamide
TFA	trifluoroacetic acid
HPLC	high pressure liquid chromatography

MALDI-TOF MS	matrix-assisted laser desorption/ionization time-of-flight mass spectrometry
DCC	*N*,*N*′-dicyclohexylcarbodiimide
NHS	N-hydroxysuccinimide
DIEA	*N*,*N*-diisopropylethylamine
ROI	region of interest.

Literature Cited

1. Hynes RO. Integrins: versatility, modulation, and signaling in cell adhesion. Cell. 1992; 69:11–25. [PubMed: 1555235]
2. Brooks PC, Clark RA, Cheresh DA. Requirement of vascular integrin alphav beta3 for angiogenesis. Science. 1994; 264:569–571. [PubMed: 7512751]
3. Friedlander M, Brooks PC, Shaffer RW, Kincaid CM, Varner JA, Cheresh DA. Definition of two angiogenic pathways by distinct alphav integrins. Science. 1995; 270:1500–1502. [PubMed: 7491498]
4. Alghisi GC, Ruegg C. Vascular integrins in tumor angiogenesis: mediators and therapeutic targets. Endothelium. 2006; 13:113–135. [PubMed: 16728329]
5. Mizejewski GJ. Role of integrins in cancer: survey of expression patterns. Proc Soc Exp Biol Med. 1999; 222:124–138. [PubMed: 10564536]
6. Stupack DG, Cheresh DA. Integrins and angiogenesis. Curr Top Dev Biol. 2004; 64:207–238. [PubMed: 15563949]
7. Cai W, Gambhir SS, Chen X. Multimodality tumor imaging targeting integrin alphavbeta3. Biotechniques. 2005; 39:S6–S17. [PubMed: 20158503]
8. Cai W, Rao J, Gambhir SS, Chen X. How molecular imaging is speeding up antiangiogenic drug development. Mol Cancer Ther. 2006; 5:2624–2633. [PubMed: 17121909]
9. Haubner R. Alphav beta3-integrin imaging: a new approach to characterise angiogenesis? Eur J Nucl Med Mol Imaging. 2006; 33(1):54–63. [PubMed: 16791598]
10. Massoud TF, Gambhir SS. Molecular imaging in living subjects: seeing fundamental biological processes in a new light. Genes Dev. 2003; 17:545–580. [PubMed: 12629038]
11. Rudin M, Weissleder R. Molecular imaging in drug discovery and development. Nat Rev Drug Discovery. 2003; 2:123–131.
12. Willmann JK, van Bruggen N, Dinkelborg LM, Gambhir SS. Molecular imaging in drug development. Nat Rev Drug Discovery. 2008; 7:591–607.
13. Kimura RH, Levin AM, Cochran FV, Cochran JR. Engineered cystine knot peptides that bind alphav beta3, alphav beta5, and alpha5 beta1 integrins with low nanomolar affinity. Proteins: Struct, Funct, Bioinf. 2009; 77:359–369.
14. Cheng Z, Wu Y, Xiong Z, Gambhir SS, Chen X. Near-infrared fluorescent RGD peptides for optical imaging of integrin alphav beta3 expression in living mice. Bioconjugate Chem. 2005; 16:1433–1441.
15. Kimura RH, Cheng Z, Gambhir SS, Cochran JR. Engineered knottin peptides: A new class of agents for imaging integrin expression in living subjects. Cancer Res. 2009; 69:2435–2442. [PubMed: 19276378]
16. Orlando RA, Cheresh DA. Arginine-glycine-aspartic acid binding leading to molecular stabilization between integrin alphav beta3 and its ligand. J Biol Chem. 1991; 266:19543–19550. [PubMed: 1717468]
17. Wu Y, Zhang X, Xiong Z, Cheng Z, Fisher DR, Liu S, Gambhir SS, Chen X. microPET imaging of glioma integrin alphav beta3 expression using ^{64}Cu-labeled tetrameric RGD peptide. J Nucl Med. 2005; 46:1707–1718. [PubMed: 16204722]

18. Kumar CC, Nie H, Rogers CP, Malkowski M, Maxwell E, Catino JJ, Armstrong L. Biochemical characterization of the binding of echistatin to integrin alphav beta3 receptor. J Pharmacol Exp Ther. 1997; 283:843–853. [PubMed: 9353406]
19. Bruning A, Runnebaum IB. CAR is a cell-cell adhesion protein in human cancer cells and is expressionally modulated by dexamethasone, TNFalpha, and TGFbeta. Gene Ther. 2003; 10:198–205. [PubMed: 12571626]
20. Pfaff M, McLane MA, Beviglia L, Niewiarowski S, Timpl R. Comparison of disintegrins with limited variation in the RGD loop in their binding to purified integrins alphaIIb beta3, alphav beta3 and alpha5 beta1 and in cell adhesion inhibition. Cell Adhes Commun. 1994; 2:491–501. [PubMed: 7538018]
21. Zhang X, Xiong Z, Wu Y, Cai W, Tseng JR, Gambhir SS, Chen X. Quantitative PET imaging of tumor integrin alphav beta3 expression with ^{18}F-FRGD2. J Nucl Med. 2006; 47:113–121. [PubMed: 16391195]
22. Wentzel A, Christmann A, Kratzner R, Kolmar H. Sequence requirements of the GPNG beta-turn of the Ecballium elaterium trypsin inhibitor II explored by combinatorial library screening. J Biol Chem. 1999; 274:21037–21043. [PubMed: 10409654]
23. Simonsen SM, Daly NL, Craik DJ. Capped acyclic permutants of the circular protein kalata B1. FEBS Lett. 2004; 577:399–402. [PubMed: 15556617]
24. de Visser M, Janssen PJ, Srinivasan A, Reubi JC, Waser B, Erion JL, Schmidt MA, Krenning EP, de Jong M. Stabilised ^{111}In-labelled DTPA- and DOTA-conjugated neurotensin analogues for imaging and therapy of exocrine pancreatic cancer. Eur J Nucl Med Mol Imaging. 2003; 30:1134–1139. [PubMed: 12768332]
25. Pless J, Bauer W, Briner U, Doepfner W, Marbach P, Maurer R, Petcher TJ, Reubi JC, Vonderscher J. Chemistry and pharmacology of SMS 201-995, a long-acting octapeptide analogue of somatostatin. Scand J Gastroenterol Suppl. 1986; 119:54–64. [PubMed: 2876507]
26. Bhushan KR, Misra P, Liu F, Mathur S, Lenkinski RE, Frangioni JV. Detection of breast cancer microcalcifications using a dual-modality SPECT/NIR fluorescent probe. J Am Chem Soc. 2008; 130:17648–17649. [PubMed: 19055348]
27. Houston JP, Ke S, Wang W, Li C, Sevick-Muraca EM. Quality analysis of in vivo near-infrared fluorescence and conventional gamma images acquired using a dual-labeled tumor-targeting probe. J Biomed Opt. 2005; 10:054010. [PubMed: 16292970]
28. Li C, Wang W, Wu Q, Ke S, Houston J, Sevick-Muraca E, Dong L, Chow D, Charnsangavej C, Gelovani JG. Dual optical and nuclear imaging in human melanoma xenografts using a single targeted imaging probe. Nucl Med Biol. 2006; 33:349–358. [PubMed: 16631083]
29. Sampath L, Kwon S, Ke S, Wang W, Schiff R, Mawad ME, Sevick-Muraca EM. Dual-labeled trastuzumab-based imaging agent for the detection of human epidermal growth factor receptor 2 overexpression in breast cancer. J Nucl Med. 2007; 48:1501–1510. [PubMed: 17785729]
30. Wang W, Ke S, Kwon S, Yallampalli S, Cameron AG, Adams KE, Mawad ME, Sevick-Muraca EM. A new optical and nuclear dual-labeled imaging agent targeting interleukin 11 receptor alpha-chain. Bioconjugate Chem. 2007; 18:397–402.
31. Zhang Z, Liang K, Bloch S, Berezin M, Achilefu S. Monomolecular multimodal fluorescence-radioisotope imaging agents. Bioconjugate Chem. 2005; 16:1232–1239.
32. Lee S, Chen X. Dual-modality probes for in vivo molecular imaging. Mol Imaging. 2009; 8:87–100. [PubMed: 19397854]
33. Cai W, Chen K, Li ZB, Gambhir SS, Chen X. Dual-function probe for PET and near-infrared fluorescence imaging of tumor vasculature. J Nucl Med. 2007; 48:1862–1870. [PubMed: 17942800]
34. Chen K, Li ZB, Wang H, Cai W, Chen X. Dual-modality optical and positron emission tomography imaging of vascular endothelial growth factor receptor on tumor vasculature using quantum dots. Eur J Nucl Med Mol Imaging. 2008; 35:2235–2244. [PubMed: 18566815]

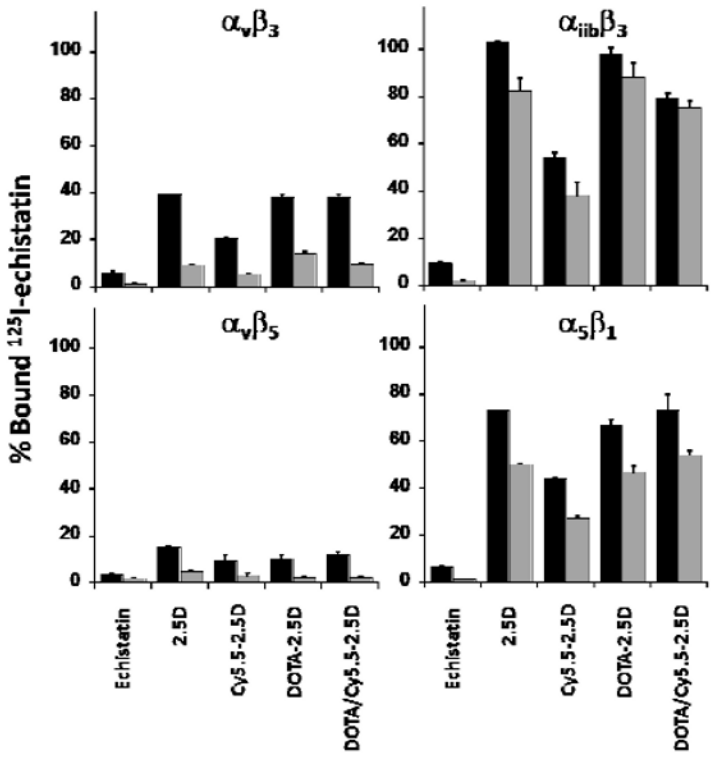

Figure 1.

Competition binding of peptides to surface-immobilized integrins. ^{125}I-labeled echistatin was allowed to compete for binding with 5 nM (black bars) or 50 nM (grey bars) unlabeled peptides to detergent-solubilized integrin receptor subtypes $\alpha_v\beta_3$, $\alpha_v\beta_5$, $\alpha_5\beta_1$, and $\alpha_{iib}\beta_3$. Unlabeled echistatin, which binds to all four integrins with high affinity, was used as a positive control. Error bars represent the standard deviation of measurements performed in triplicate.

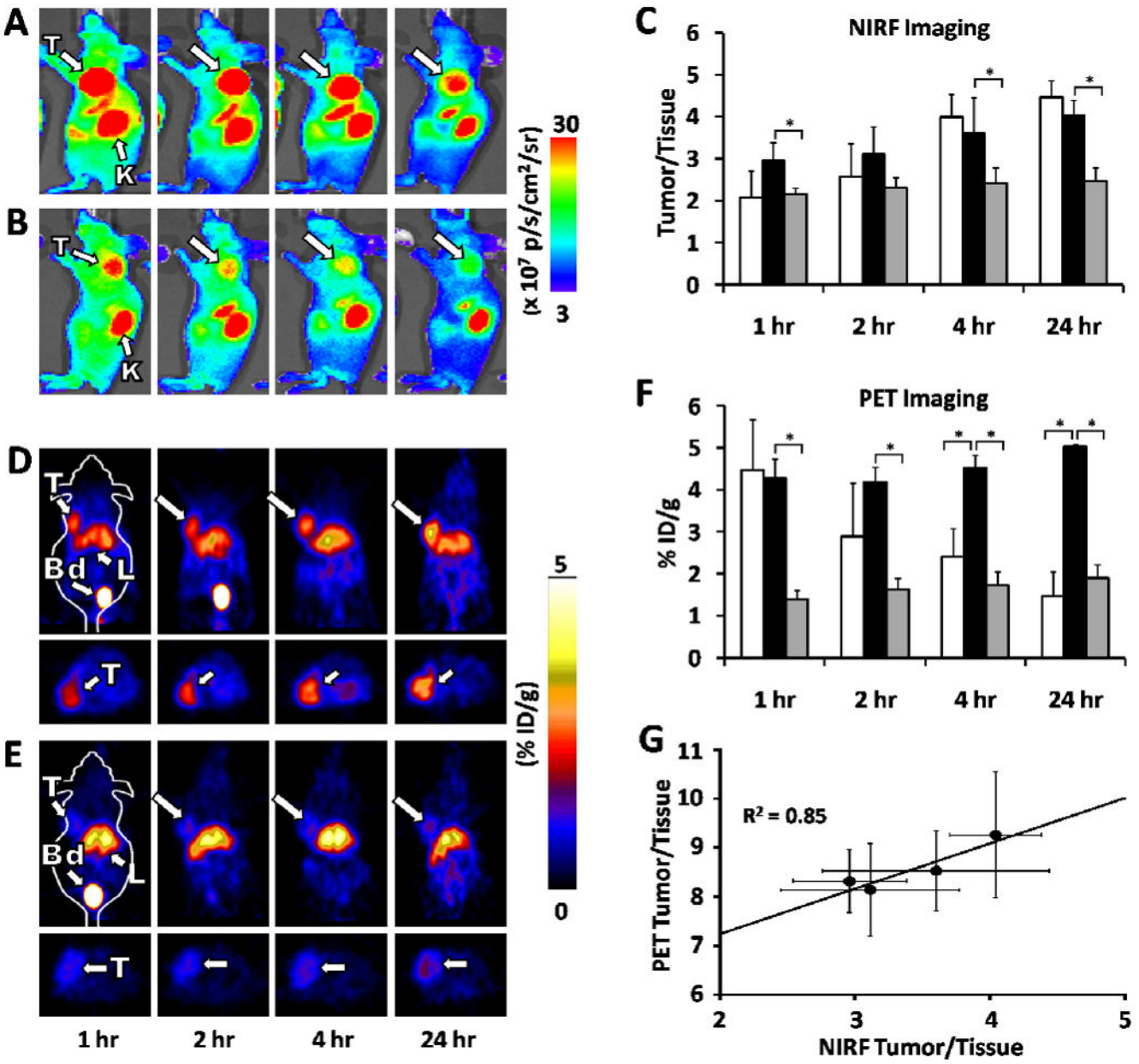

Figure 2.

NIRF and microPET imaging of knottin probes in murine human tumor xenograft models. Mice bearing U87MG tumors were injected via tail vein with either (A) 1.5 nmol of DOTA/Cy5.5-2.5D, or (D) ~ 100 μCi of ^{64}Cu-DOTA/Cy5.5-2.5D. For blocking experiments (B, E), mice were co-injected with an excess (0.5 μmol) of unlabeled c(RGDyK) in addition to labeled knottin peptides. Representative images are shown at 1, 2, 4, and 24 hr post injection. T= tumor; K= kidney; Bd= bladder; L= liver. (C) NIRF imaging, represented as the tumor-to-background tissue (Tumor/Tissue) ratio for Cy5.5-2.5D (white bars), DOTA/Cy5.5-2.5D (black bars), and DOTA/Cy5.5-2.5D plus excess unlabeled c(RGDyK) blocking peptide (grey bars). (F) MicroPET imaging, quantified as the % ID/g of ^{64}Cu-DOTA-2.5D (white bars) ^{64}Cu-DOTA/Cy5.5-2.5D (black bars), and ^{64}Cu-DOTA/Cy5.5-2.5D plus an excess of unlabeled c(RGDyK) blocking peptide (grey bars). Error bars represent the SD of

measurements performed on at least three mice. (G) Correlation analysis of average tumor to background tissue ratios for NIRF and microPET images acquired at 1, 2, 4, and 24 hr post injection. Error bars represent the SD of measurements in three mice. (* $p < 0.05$).

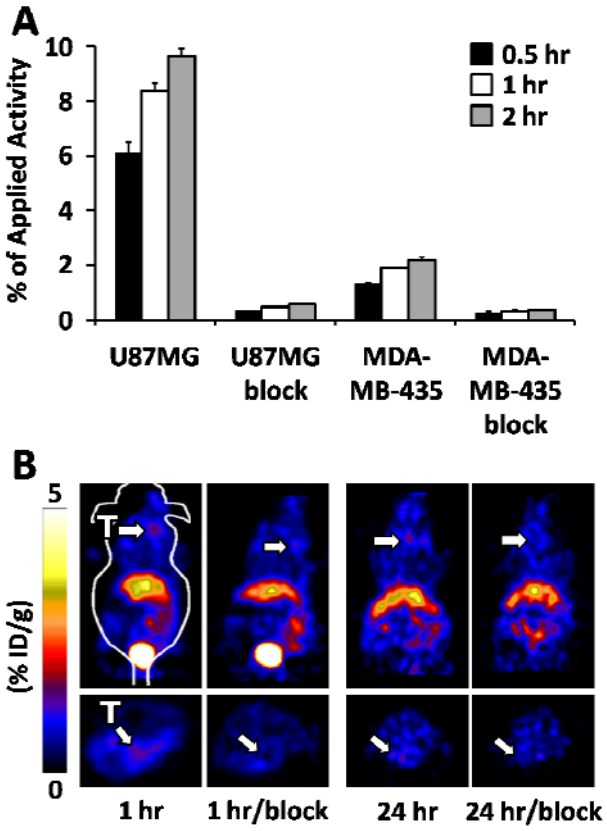

Figure 3.

Uptake and imaging in MDA-MB-435 cells and xenograft tumors. (A) Uptake of ^{64}Cu-DOTA/Cy5.5-2.5D in U87MG or MDA-MB-435 cells at 0.5, 1, and 2 hr. Blocking studies, indicated by “block”, were performed in parallel using a large molar excess of c(RGDyK). (B) MicroPET images of mice bearing subcutaneous MDA-MB-435 tumors at 1 hr and 24 hr post injection. Blocking experiments with unlabeled c(RGDyK) were performed to further demonstrate probe specificity.

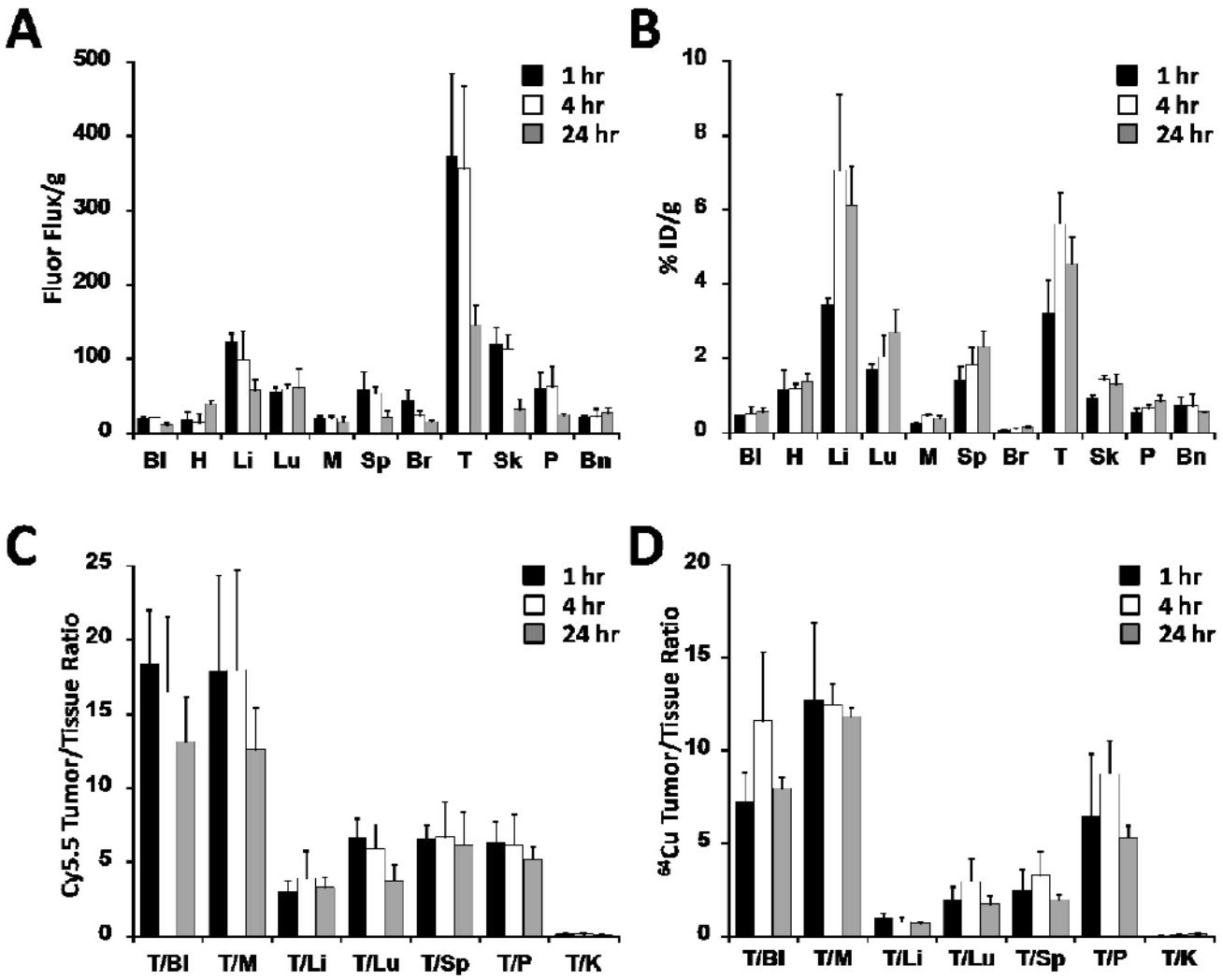

Figure 4.

Comparison of Cy5.5 and ^{64}Cu tissue biodistribution. The amount of (A) DOTA/Cy5.5-2.5D or (B) ^{64}Cu-DOTA/Cy5.5-2.5D accumulation was measured in the blood (Bl), heart (H), liver (Li), lung (Lu), muscle (M), spleen (Sp), brain (Br), tumor (T), skin (Sk), pancreas (P), and bone (Bn). (A) Cy5.5 uptake, measured as the fluorescence flux (photons per second) per gram of tissue. (B) ^{64}Cu uptake, quantified as the %ID/g. Comparison of Tumor/Tissue ratios observed at 1, 4, and 24 hr post injection for (C) DOTA/Cy5.5-2.5D or (D) ^{64}Cu-DOTA/Cy5.5-2.5D.

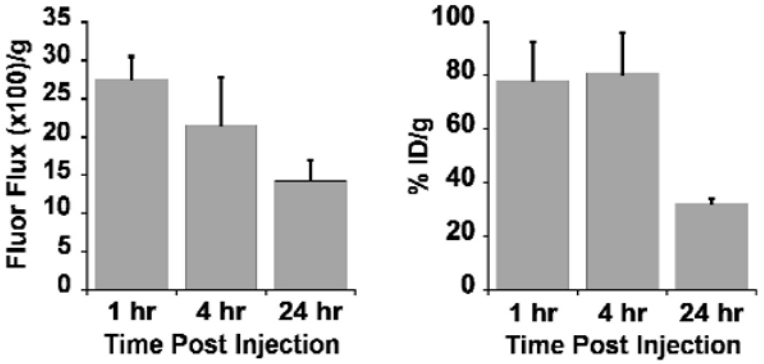

Figure 5.

Comparison of Cy5.5 and ^{64}Cu accumulation in the kidney. Uptake of Cy5.5 resulting from injection of DOTA/Cy5.5-2.5D (left panel) was measured as the fluorescence flux (photons per second) per gram of tissue. Uptake of ^{64}Cu-DOTA/Cy5.5-2.5D (right panel) was quantified as the %ID/g.

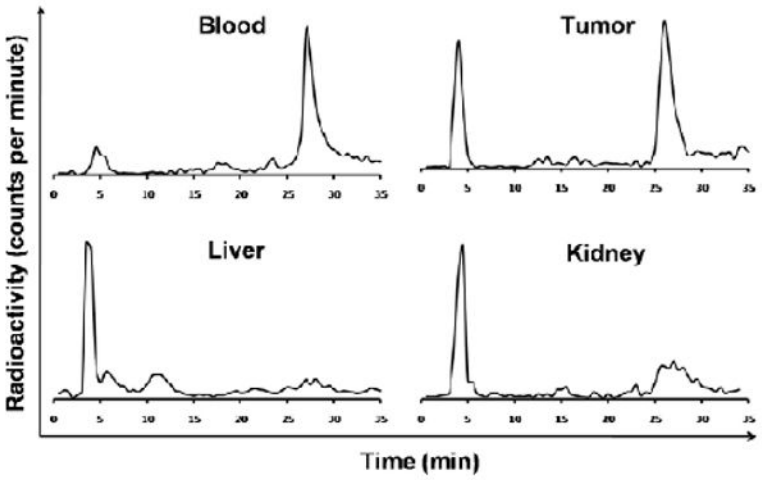

Figure 6.

In vivo metabolic stability of ^{64}Cu-DOTA/Cy5.5-2.5D. Homogenized tissues were analyzed by radio-HPLC and gamma counting 1 hr post injection. The intact radiotracer elutes at around 27 minutes.

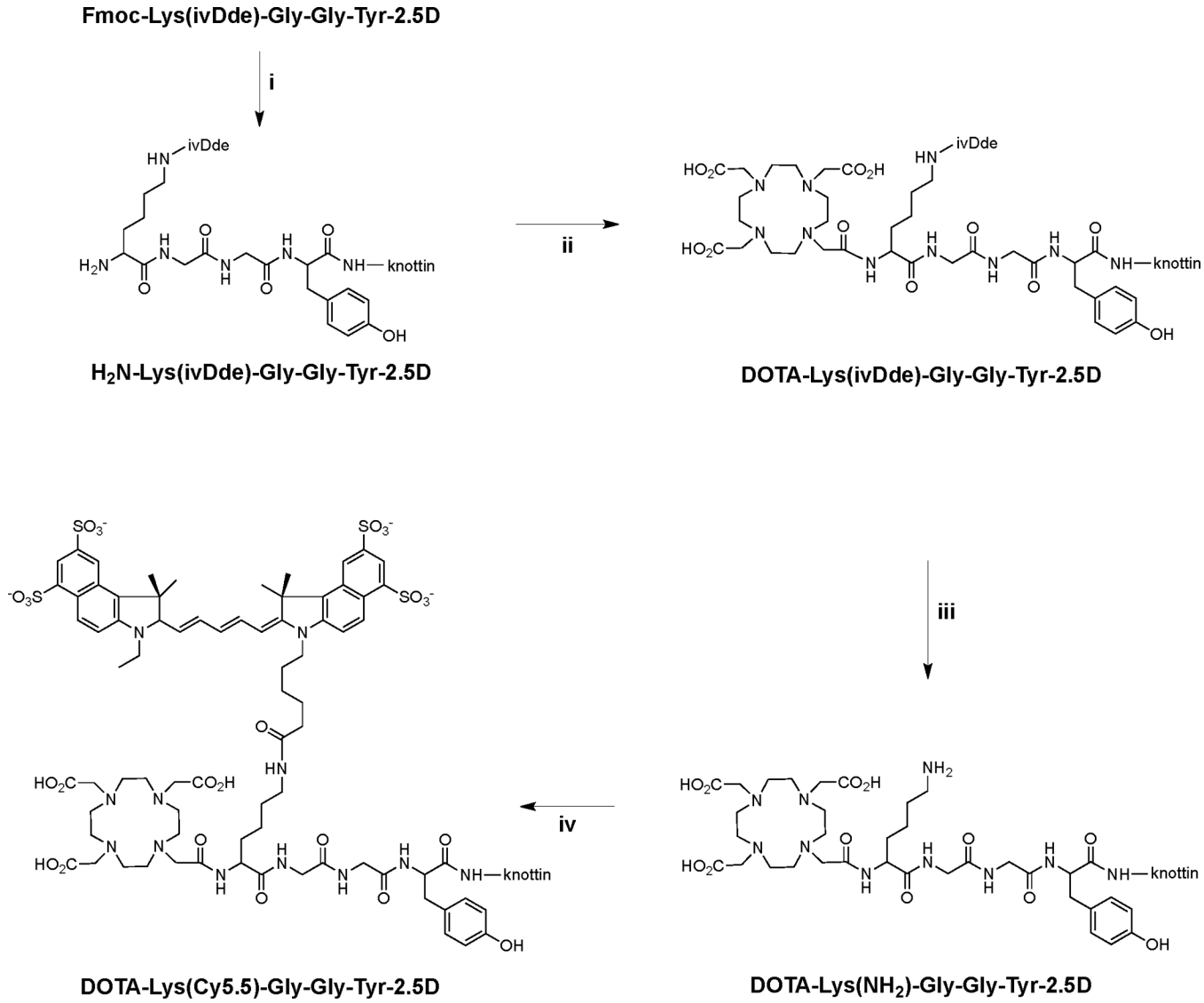

Scheme 1.

Chemical conjugation of DOTA and Cy5.5 to knottin peptide 2.5D. The peptide-based crosslinker Fmoc-Lys(ivDde)-Gly-Gly-Tyr was first synthesized and coupled to the N-terminus of the folded knottin peptide 2.5D using succinimide ester activation chemistry. Next, the Fmoc group was removed from the N-terminus of the crosslinker (i: 10% piperidine/DMF, 0.5 hr, RT), and the resulting compound was reacted with a 5-fold molar excess of an NHS ester-activated DOTA group (ii: DMF/2% DIEA, 0.5 hr, RT) to generate DOTA-Lys(ivDde)-Gly-Gly-Tyr-2.5D. Finally, the ivDde group was removed from the ε-amino group of Lys (iii: 2% hydrazine/DMF, 0.5 hr, RT) and the resulting compound was reacted with Cy5.5 NHS ester (iv: DMF/2% DIEA, 0.5 hr, RT) to give the final product: DOTA-Lys(Cy5.5)-Gly-Gly-Tyr-2.5D, which was used for NIRF imaging experiments, or radiolabeled with ^{64}Cu and used for PET imaging experiments.

Table 1

U87MG cell binding data, reported as IC_{50} values

Ligand	IC_{50}
Echistatin	4 ± 1 nM*
Knottin 2.5D	19 ± 6 nM
Cy5.5-2.5D	5 ± 1 nM*
DOTA-2.5D	9 ± 3 nM*
DOTA/Cy5.5-2.5D	30 ± 7 nM

* Difference compared to DOTA/Cy5.5-2.5D is statistically significant ($p < 0.05$)